Transport by intermittency in the boundary of the DIII-D tokamak[a)]

J. A. Boedo,[1,b)] D. L. Rudakov,[1] R. A. Moyer, G. R. McKee,[2] R. J. Colchin,[3] M. J. Schaffer,[4] P. G. Stangeby,[5] W. P. West,[4] S. L. Allen,[6] T. E. Evans,[4] R. J. Fonck,[2] E. M. Hollmann,[1] S. Krasheninnikov,[1] A. W. Leonard,[4] W. Nevins,[6] M. A. Mahdavi,[4] G. D. Porter,[6] G. R. Tynan,[1] D. G. Whyte,[1] and X. Xu[6]

[1]*University of California, San Diego, Energy Research Center and Mechanical and Aerospace Engineering Department, La Jolla, California 92093*
[2]*University of Wisconsin, Madison, Wisconsin 53706*
[3]*Oak Ridge National Laboratory, Oak Ridge, Tennessee*
[4]*General Atomics, San Diego, California*
[5]*University of Toronto, Toronto, Canada*
[6]*Lawrence Livermore National Laboratory, Livermore, California*

(Received 13 November 2002; accepted 3 February 2003)

Intermittent plasma objects (IPOs), featuring higher pressure than the surrounding plasma, are responsible for ~50% of the $E\times B_T$ radial transport in the scrape off layer (SOL) of the Doublet III D (DIII-D) tokamak [J. L. Luxon, Nucl. Fusion **42**, 614 (2002)] in *L*- and *H*-mode discharges. Conditional averaging reveals that the IPOs are positively charged and feature internal poloidal electric fields of up to 4000 V/m. The IPOs move radially with $E\times B_T/B^2$ velocities of ~2600 m/s near the last closed flux surface (LCFS), and ~330 m/s near the wall. The IPOs slow down as they shrink in size from 2 cm at the LCFS to 0.5 cm near the wall. The skewness (i.e., asymmetry of fluctuations from the average) of probe and beam emission spectroscopy data indicate IPO formation at or near the LCFS and the existence of positive and negative IPOs which move in opposite directions. The particle content of the IPOs at the LCFS is linearly dependent on the local density and decays over ~3 cm into the SOL while their temperature decays much faster (~1 cm).
 [DOI: 10.1063/1.1563259]

I. INTRODUCTION

Recent evidence[1–3] indicates that the far scrape-off layer (SOL) density and temperature profiles in various tokamaks and other devices are often nonexponential and flat, enhancing the plasma–wall contact beyond what would be expected from exponential profiles and suggesting that perpendicular transport in these conditions is much larger than expected.

A candidate for the additional edge/SOL transport, intermittency in the fluctuations corresponding to events above the standard deviation, has been extensively documented in linear devices,[4,5] stellarators,[6] and tokamaks[7–9] and its statistical properties examined[10,11] via the probability distribution function[12] (PDF). The fluctuations depart from a Gaussian distribution, featuring large skewness[12] and kurtosis[12] due to the intermittent events. Furthermore, it has been proven that the statistical properties of the fluctuations are alike and near-Gaussian in the shear layer while deviating from Gaussian into the SOL[13] of tokamaks [Joint European Torus (JET[14])], and stellarators[15] (Advanced Toroidal Facility, ATF,[15] Weldestein 7 Advanced Stellarator W7-AS[16]). The intermittency has been analyzed using conditional averaging tools in both linear devices[4,5] and tokamaks,[17,18] with the result that coherent structures propagating radially are responsible for much of the radial transport. Comparative work at the devices TJ-I[19] and TJ-IU[20] concluded that intermittency bears a substantial part of the transport and most importantly, that the various properties of the intermittency (power spectra, PDF moments, etc.) are self-similar in tokamaks and torsatrons. Work in the JET tokamak[21] focused on the power spectra of the fluctuations, demonstrating that its decay as $1/f$ was localized in the spectral region where intermittent transport is dominant and interpreting the result as an indication of closeness to instability thresholds. On the other hand, very recent work[22–24] on the Alcator-C[25] device has mostly focused on transport analysis of the SOL and demonstrated the need for very large diffusion coefficients if convection is not considered. Additionally, there is an extensive body of work imaging the edge of various devices with fast cameras[24,26] which show that moving plasma filaments exist in the edge/SOL. However, although the preponderance of intermittency and the concomitant fast convective transport in confined plasmas has been established,[4,6,21] no detailed work on the dynamical characteristics and origin or on the scaling with plasma parameters has been done until the present work.

We build on recent work[27–29] and present here data from DIII-D showing that the fast, intermittent, convective radial transport in the DIII-D SOL results in plasma parameters with non-Gaussian fluctuation statistics featuring rich radial structures that partly correspond to the simultaneous presence of both positive and negative intermittent events in a narrow region near or at the separatrix. The results of a density scan in *L* mode are also shown indicating that the particle content of the intermittent events and their frequency

[a)]Paper KI2 2, Bull. Am. Phys. Soc. **47**, 183 (2002).
[b)]Invited speaker.

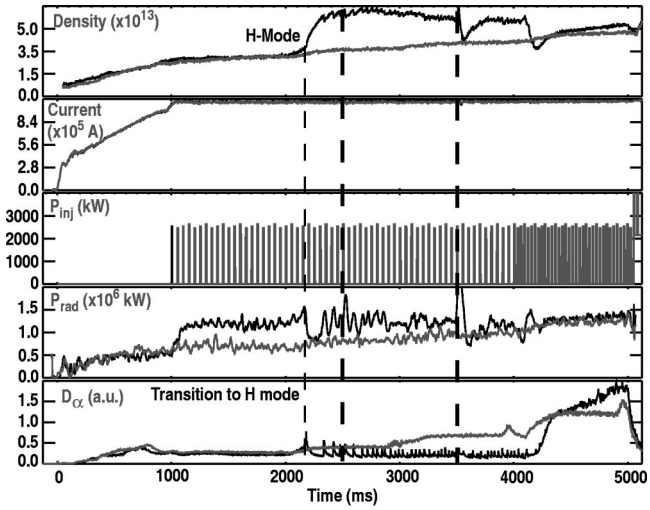

FIG. 1. Time evolution of two discharges in DIII-D showing from top to bottom, density, plasma current, injected power, radiated power, and D_α signals. The transition to H mode occurs at 2.15 s in one of the discharges (black lines) as indicated by the leftmost vertical line. The probe is inserted at the times marked by the two thick rightmost vertical lines.

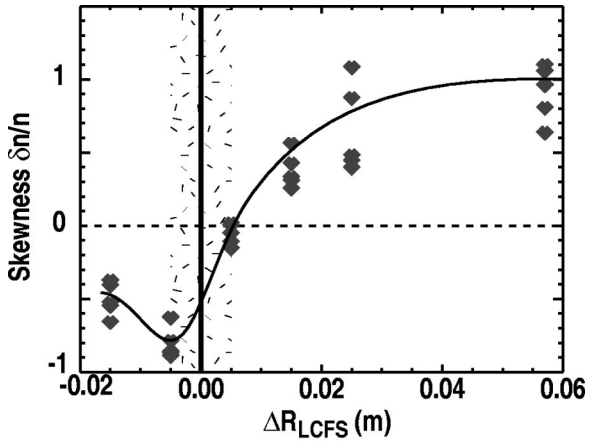

FIG. 3. The skewness of the density signal from BES shows marked deviation from Gaussian behavior in the SOL and the presence of negative bursts near the LCFS.

increase with the local density. Radial transport and thus the plasma–wall contact are enhanced by the intermittent transport. Although the source of the intermittency is not addressed in this paper, we present strong evidence that the phenomena occur at/near the last closed flux surface (LCFS). These findings provide a strong motivation to further investigate the conditions under which large cross-field convective transport exists in the SOL.

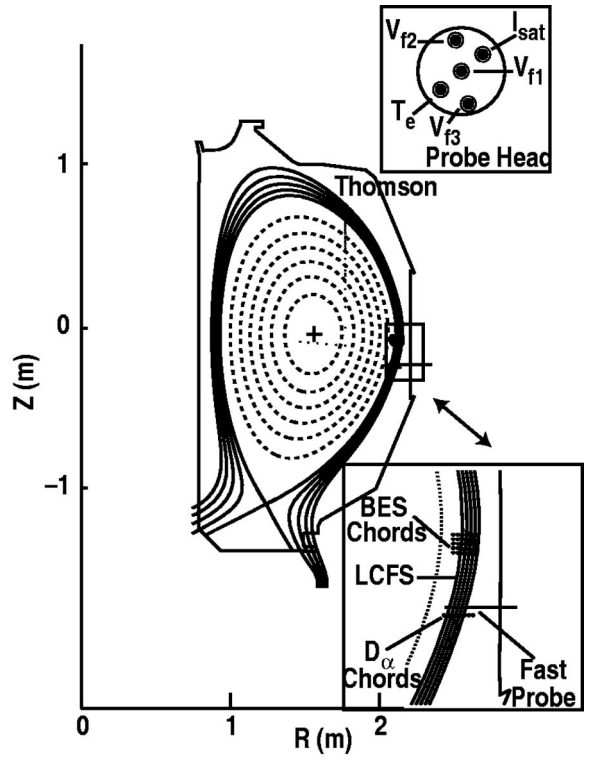

FIG. 2. Poloidal cut of DIII-D showing the magnetic geometry and some relevant diagnostics. Two insets show (top) the scanning probe tip geometry and (bottom) the BES diagnostic geometry. The Thomson scattering chords are indicated at the top.

II. EXPERIMENTAL SETUP

The experiments were carried out on the DIII-D tokamak[30,31] in a variety of discharges with plasma current $I_p = 1.0$ MA and toroidal field of $B_T = 2.0$ T at the major axis, $R = 1.7$ m. Discharges with neutral beam heating power of up to 2 MW, featuring both low (L) and high (H) confinement modes, with double- and single-null divertor geometry (at the bottom of the vacuum vessel) and with standard and reversed B_T directions were investigated. Otherwise identical H- and L-mode discharges, shown in Fig. 1, were analyzed in particular detail for comparative studies. In some discharges, the density was increased in a stepwise manner from $\langle n_e \rangle / n_{GW} = 0.26$ to 0.6, as shown in Figs. 1 and 8, while a reciprocating probe at the midplane (Fig. 2) was inserted at various times, illustrated by the vertical lines in Fig. 1, to assure coverage at various densities.

The principal measurements were made by a fast scanning probe array[32] featuring five tips (Fig. 2 upper inset) that sense Langmuir probe current I, saturation current, I_{sat}, and floating potential, V_f. The measured ion saturation current, I_{sat}, given by the expression $I_{\mathrm{sat}} = (1/2) A_{\mathrm{pr}} e n_e c_s = (1/2) A_{\mathrm{pr}} e n_e [k(T_e + T_i)/m_i]^{1/2}$ (T_e and T_i are the ion and electron temperatures, respectively, A_{pr} is the tip area, and n_e is the electron density) allows calculation of the electron density if T_e is known (assuming $T_e = T_i$). One tip functions as a fast T_e diagnostic,[33] using current excitation about the floating potential with bandwidth of 150 kHz, and thus is able to resolve the temperature inside the structures. These measurements were combined to infer the electron density n_e, by using the above-given equation, and the poloidal electric field, $E_\theta = (V_{f1} - V_{f2})/\delta\theta$, for probe tips separated a distance $\delta\theta$. Time resolution down to 1.0 μs has been achieved. The probe scans 15.2 cm horizontally from the outside wall in approximately 250 ms along the path indicated in Fig. 2. The calculation of E_θ assumes that the temperature and sheath drop are identical in both tips and that the intermittent objects are larger than the separation between the tips. The

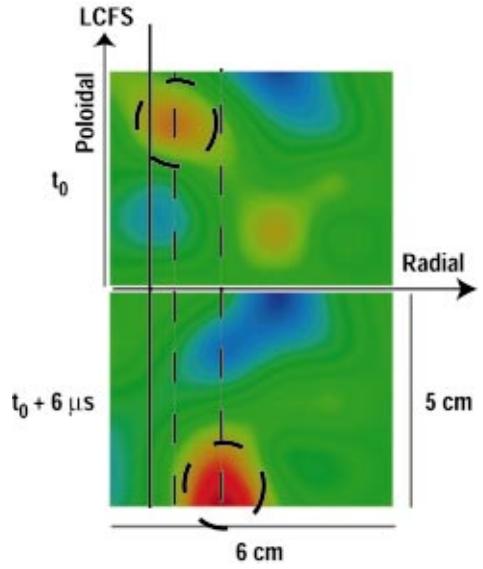

FIG. 4. (Color) Two frames from BES showing 2-D density plots. There is a time difference of 6 μs between frames. Red indicates high density and blue low density. A structure, marked with a dashed circle and shown in both frames, features poloidal and radial motion.

last assumption is justified later using beam emission spectroscopy (BES) data. The plasma potential V_p was calculated as $V_p \sim V_f + 3.0kT_e$. The D_α sensor array, also shown in Fig. 2, provided independent, radially resolved (1 cm) signals at 10 μs resolution. The BES system, which measures density and its fluctuations, was configured as a 5×6 fiber array as seen in Fig. 2, and was located at the edge of the plasma in the midplane to provide fast (1 μs) two-dimensional (2-D) imaging of the density. The measurements are mapped onto the magnetic surfaces, displayed in Fig. 2, calculated by the toroidal equilibrium fitting code EFIT.[34]

III. GENERAL DESCRIPTION OF THE INTERMITTENCY

Intermittency, i.e., occasional bursts in a signal, is quite evident in many edge diagnostics in tokamaks. If the bursts occur preferentially in one direction, i.e., bursts are mostly positive in I_{sat}, an asymmetry is conveyed to the various signals that affects their statistical characteristics and introduces a deviation from the Gaussian distribution. The deviation translates into a skewness[12] (i.e., positive n_e bursts generate positive skewness) of ~1 (a Gaussian distribution would feature a skewness of zero) in the SOL density signals, as shown in Fig. 3. Signal statistics for both the *L* and *H* mode show significant and similar skewness in the SOL. It is crucial to notice that the skewness changes sign at or near the LCFS,[27] within the error bars of EFIT, indicating that negative events are present, corresponding to drops in the density signal from its average level.

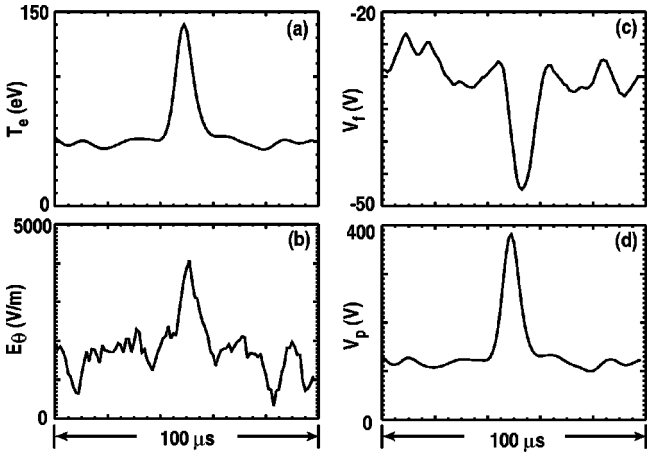

FIG. 5. Conditional average results for (a) T_e, (b) E_θ, (c) V_f, (d) V_p showing that (1) the plasma structures are charged positively, (2) contain and convect substantial amounts of energy, and (3) a positive radial electric field exists inside them.

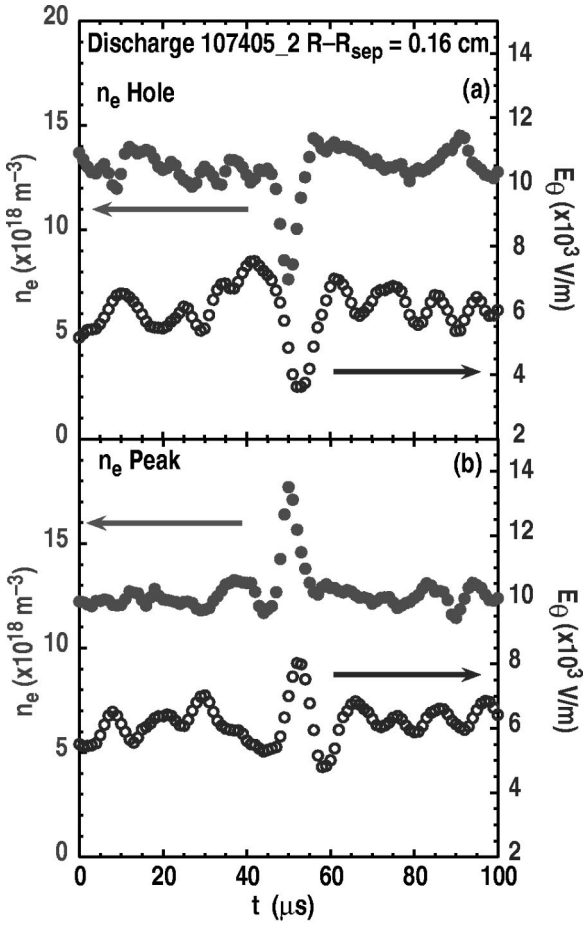

FIG. 6. Conditional averaging reveals that both positive and negative IPOs exist at/near the LCFS. However, the opposite signs of the measured E_θ indicate that the negative IPOs travel inwards toward the core while the positive IPOs propagate into the SOL.

The intermittency in the density can be visualized by comparing two frames (2-D images) from BES, separated in time by 6 μs as shown in Fig. 4, where the LCFS is indicated by a solid vertical line. High density is indicated in red and low in blue. The radial motion of a positive density feature, marked by a dashed circle in both frames, is indicated by vertical dashed lines. Notice that the object has a radial and poloidal spatial extent of roughly 2 cm. From the two frames it is clear that the object is moving poloidally and radially

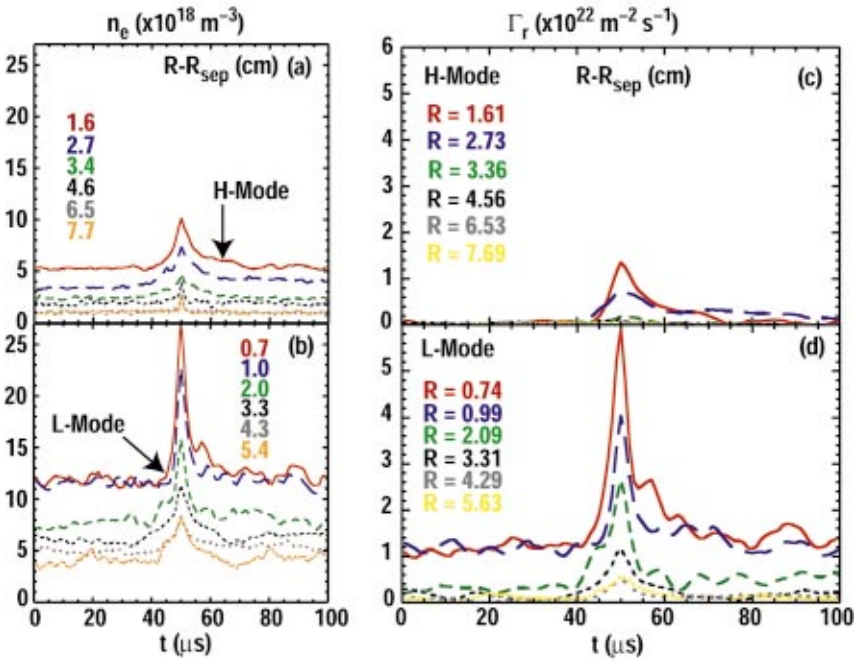

FIG. 7. (Color) Density of the IPOs is compared for *H* mode (a) and *L* mode (b). Particle flux due to the intermittency is compared for *H* mode (c) and *L* mode (d). In general, intermittency has a higher amplitude in *L* mode.

with speeds that can be easily estimated at $V_\theta = 5$ km/s and $V_r = 1.5$ km/s. These compare well to Langmuir probe results.

To separate these coherent objects from other fluctuations, standard conditional averaging tools, introduced in the TEXT tokamak by Filippas[17] and later in various devices,[4,5] were used to quantify the observations. A 2.5×rms-level threshold was used to discriminate the intermittent events in 5-ms-long time series of I_{sat}. These were then binned for 100 μs about the maximum of each event, accumulated and averaged, producing the results seen in Fig. 5. The conditional averaging tool, applied to I_{sat} with the parameters described, corresponds to ~40 events at the LCFS. The selected time windows result on averaging over frequencies higher than those associated to the time scale of the binning window (or correspondingly, to structures that are smaller than the selected scale, which is in this case ~2 cm). Lower frequencies or larger spatial scales than the selected windows will appear as a dc offset in the averaged data. The existence of an event in I_{sat} is used as the condition to select time slices in the E_θ and V_f signals at the same time. From the measurement of E_θ, a radial velocity, $V_r = (E_\theta \times B/B^2)$ can be inferred and, knowing the time ∂t that the perturbation appears in the probe tips, a radial size, $\partial r = \partial t V_r$ can be calculated. The results, published previously,[27] indicate that the objects shrink in size from ~2 cm at the LCFS to ~0.2 cm in the far SOL.

The results from conditional averaging of the T_e trace, shown in Fig. 5, indicate that the temperature in the intermittent plasma objects (IPOs) [Fig. 5(a)] is 150 eV, nearly three times that of the background (50 eV) and their potential [Fig. 5(d)], calculated as $V_p \approx V_f + 3kT_e$ [V_f shown in Fig. 5(c)], is 400 V and positive with respect to the surrounding plasma (120 eV), suggesting that a predominant electron loss occurs at the IPO boundaries. Furthermore, the burst in plasma potential shown in Fig. 5(d) indicates that the IPOs (with dimensions of roughly 3 cm×3 cm in the poloidal plane) contain an internal radial electric field, $E_r = -\nabla V_p$, that can be estimated as $E_r \approx \Delta V_p / \delta r = 200$ V/cm and results in internal rotation at a $V_{\theta'} = E_{r'}/B_T$ speed of 1.33×10^4 m/s. These structures, therefore, possess positive vorticity. In the above-noted measurements, the only assumption is that we can resolve the temperature in these objects fast enough and that the plasma potential can be calculated as $V_p \approx V_f + 3kT_e$.

Furthermore, conditional averaging performed on the probe data near the LCFS, and shown in Fig. 6, agree with the skewness data (Fig. 3) by showing the presence of *both* positive and negative events. These events are comparable in size, indicating that the local density profile experiences bursts and dips that fuse, break, and mix in this narrow region at the LCFS. This results in the skewness, a measure of asymmetry in the probe and BES signals, data going to zero. Furthermore, the E_θ data also show (Fig. 6) that while the positive events proceed to move into the SOL with velocity $V_r = (E_\theta \times B/B^2)$, the negative ones move inward toward the core, as has recently been predicted.[27] Important implications of this result are that (1) the edge plasma is being diluted by the lower density events moving inward and (2) the negative events can move impurities into the plasma core.

IV. *L–H* MODE COMPARISON

Results from conditional averaging of probe data from otherwise identical *L*- and *H*-mode discharges (Fig. 1) showing the typical (average) IPOs are shown in Figs. 7(a) and 7(b) by superimposing traces from various radii and indicating (arrow) the direction of increasing radius. The *H*-mode discharges used in these experiment are close to the *L–H* threshold and, therefore, are not high performance *H*-mode discharges, where the SOL transport is further suppressed.

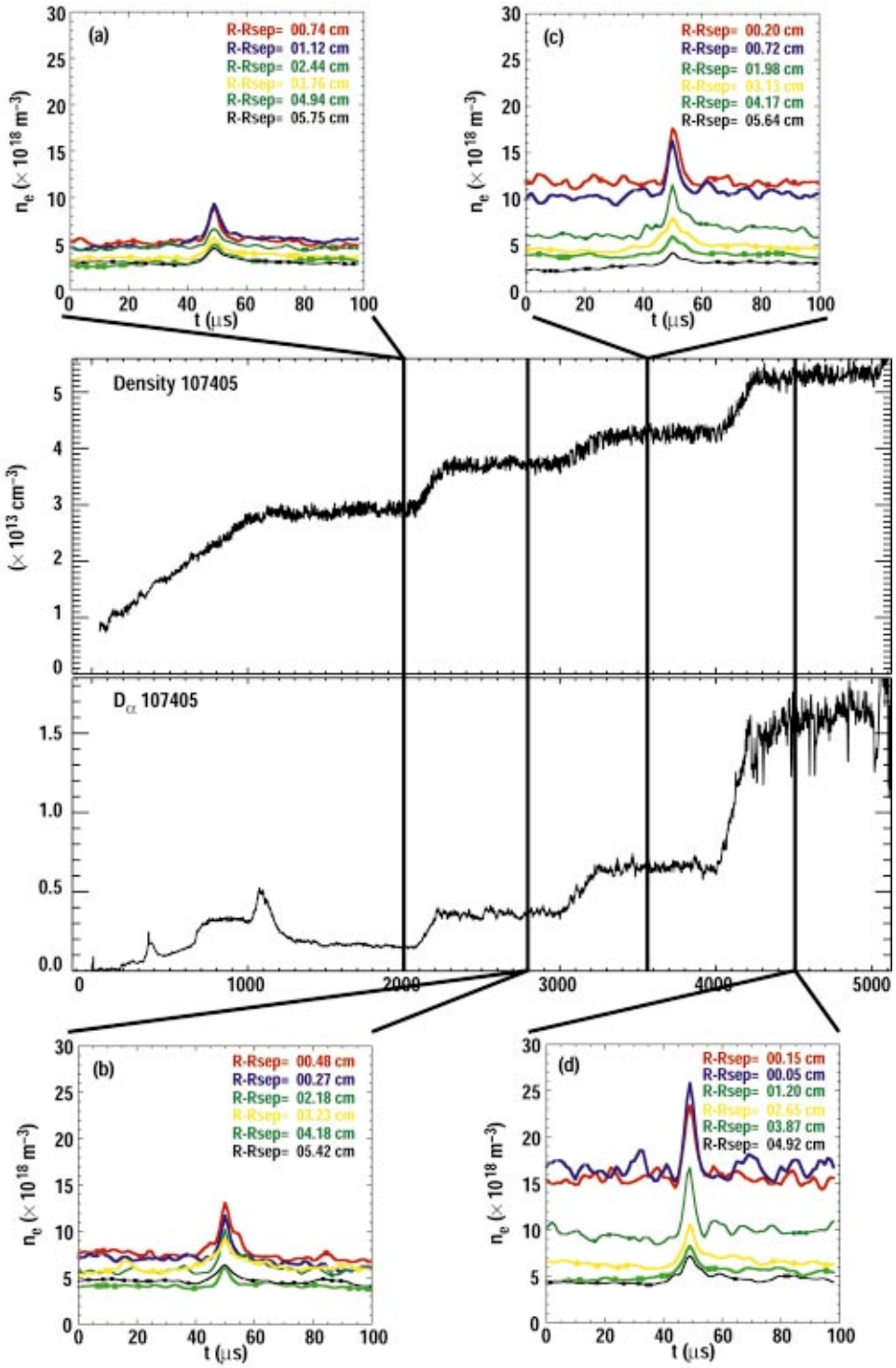

FIG. 8. (Color) *L*-mode discharges where the density was increased stepwise (central frame) allow comparison of IPO density vs discharge/edge density (insets) and a relation of proportionality is found.

Three properties of the data are immediately apparent: (1) the density excursion is two to three times the background density, (2) the amplitude of the pulses for similar radius is much larger for *L*-mode conditions than for *H*-mode conditions, and (3) the amplitude of the pulses decays rapidly with radius. Evaluation of the total particle flux convected by the IPOs is of utmost importance to assess their relevance to the radial transport. The flux can be calculated as $\Gamma_{\text{int}} = n_e(E_\theta \times B/B^2)$ and the result is shown in Figs. 7(c) and 7(d) for *L*- and *H*-mode conditions using the same vertical scale in both plots. Three properties are again quite apparent: (1) the flux excursion is large and nearly five times the background, (2) the flux for similar radius is much larger for *L*-mode conditions than for *H*-mode conditions, and (3) the flux decays rapidly with radius.

The relevance of the IPOs to total $E \times B$ radial transport in the SOL is obtained in *L* and *H* mode at various radii by calculating

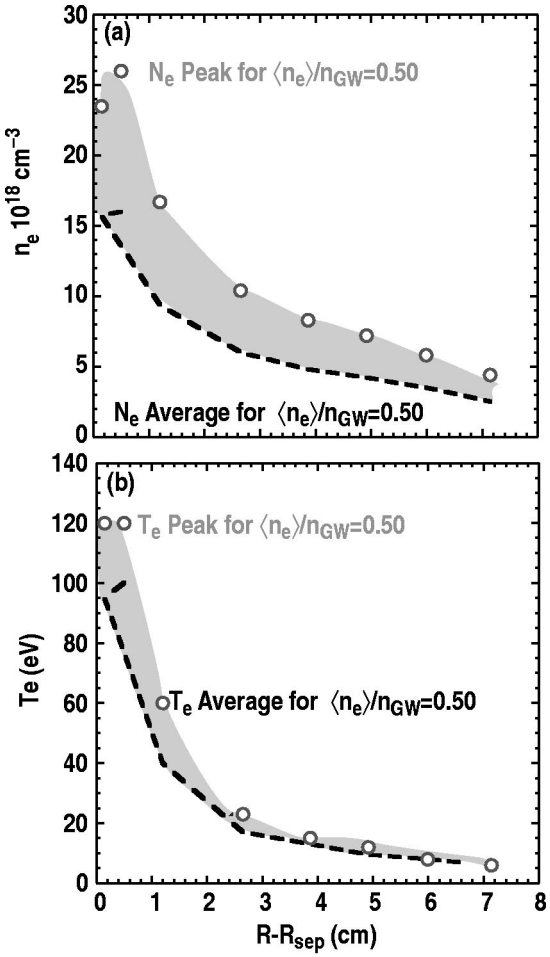

FIG. 9. Radial profiles of (a) the IPO peak density from conditional averaging (circles) and the average density profile (line) and (b) the IPO peak temperature (circles) and the average temperature profile (line). The peak IPO density decays with the same scale length as the background profile while the peak temperature decays much faster.

$$\Gamma_{\text{intermittent}}/\Gamma_{\text{total}} = \langle n_e (E_\theta \times B/B^2) \rangle_{\text{intermittent}} / \langle n_e (E_\theta \times B/B^2) \rangle_{\text{total}}.$$

The results indicate that: (a) intermittent events above the 2.5×rms level are responsible for ~50% of the transport *at all radii where we have measurements*, (b) there is a continuum of event sizes, and (c) although the relative relevance of intermittency is unchanged with radius, its absolute amplitude decays rapidly with radius due to the decay of the structures themselves.

It is important to notice that the intermittency under study here, residing in the 1–200 kHz band, is part of the $E \times B$ electrostatic turbulent particle flux, $\tilde{\Gamma}_r$, that depends on the rms value of the density, $\langle \tilde{n}_e^2 \rangle^{1/2}$, poloidal field, $\langle \tilde{E}_\theta^2 \rangle^{1/2}$, and their cross-correlation. Since $\tilde{\Gamma}_r$ has been characterized extensively in many devices[35–38] and in particular, DIII-D,[39] the Texas Experimental Tokamak[40] (TEXT),[41–42] and the Torus Experiment for Technology Oriented Research[43] (TEXTOR)[44,45] it can therefore be stated that the general properties of the intermittency, such as its response to sheared electric fields that decorrelate turbulent transport resulting in reduced transport and enhanced confinement conditions, have been indirectly characterized.

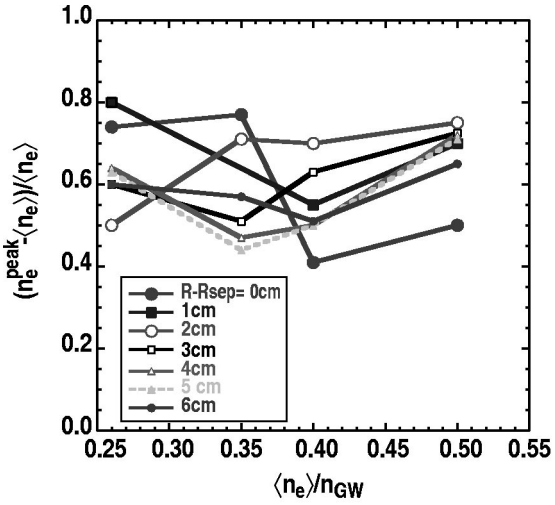

FIG. 10. The normalized intensity of the IPO density for various radiis features independence from the discharge density (in $\langle n_e \rangle / n_{GW}$ units).

V. *L*-MODE DENSITY SCALING

Since the interaction of the plasma with the far wall has been reported to increase with discharge density,[22] and the IPOs can provide a mechanism for fast convection of particles, it is of interest to explore the scaling of the IPO properties. *L*-mode discharges with density steps from $\langle n_e \rangle / n_{GW} = 0.25$ to 0.6 were chosen due to the prominence of the intermittency and the absence of edge localized modes (ELMs). Conditional averaging was applied to the probe data for the various density steps and the results are displayed in Fig. 8, The radial dependency over ~5 cm is also shown by superimposing traces as before. As the discharge density is

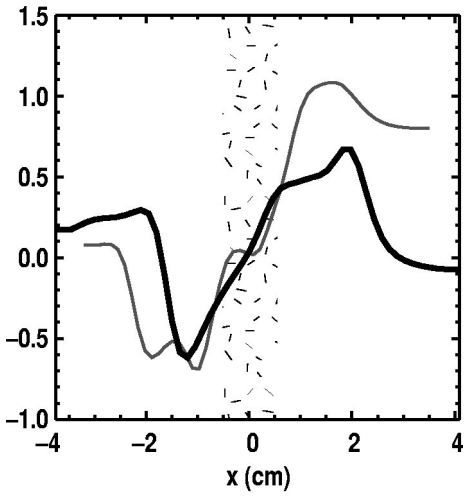

FIG. 11. Profiles of skewness for low (red) and high (black) densities in *L*-mode conditions. The skewness crosses zero near the LCFS and toward the core and it is high elsewhere. Negative skewness indicates negative IPOs.

increased, the IPO density, displayed in the insets of Figs. 8(a)–8(d), also increases. Thus the density of the IPOs scales with the discharge/edge density.

The IPOs decay as they travel into the SOL. It is thus important to address the question of how fast the decay is, and conditional averaging was applied to density and temperature data with ~1 cm radial resolution. Radial profiles of the averaged (line) and IPO peak (dots) density/temperature are shown in Figs. 9(a) and 9(b) for *L*-mode conditions and their difference highlighted. It can be noted in Fig. 9(a) that the peak IPO density is about 70% of the background density and both decay with radius with a decay length, L_n, of 2.7 cm. Quite different behavior is seen on the temperature, where the IPO peak temperature decays to that of the background profile within 1 cm. Therefore, the IPOs quickly thermalize with the background.

The relative importance of the IPO density can be evaluated as a function of $\langle n_e \rangle / n_{GW}$ by calculating the IPO intensity $[n_e^{\text{peak}} - \langle n_e^{\text{aver}} \rangle] / \langle n_e^{\text{aver}} \rangle$ for various radii in the SOL, as shown in Fig. 10. Despite the fact that the particle content (or density excursion) of the IPOs increases with density (as seen in Fig. 8), the IPOs' relative contribution to the density is fairly constant with radius and density at about 50%–70%. These results indicate a scaling of the IPO intensity with transport. The decay of the IPOs can be understood in light of recent analytical work[46–48] where they are modeled as structures elongated along the magnetic field which are being drained at the divertor plates. The IPO density and temperature is predicted to be

$$n(r,t) = n(r)/(1 + t/\tau_T)^{2\alpha/\alpha_T} \tag{1}$$

and

$$T(t) = T_0/(1 + t/\tau_T)^2, \tag{2}$$

where $\alpha_T = \alpha S_E$; $\tau_T = 2/(\alpha_T T_0^{1/2})$, α measures the net parallel current to the divertor plates, S_E is the sheath energy transmission factor, and T_0 is the temperature of the IPO as it detaches from the LCFS. Since $2\alpha/\alpha_T = 2/S_E \ll 1$, comparison of Eqs. (1) and (2) shows that the temperature decays much more rapidly in time than the density, just as observed in the experiment. The quick reduction in the amplitude of the bursts and density profiles is, therefore, in agreement with a strong sink in the divertor.

VI. PROGRESS ON THEORETICAL UNDERSTANDING

Efforts to understand the intermittency and its implication for radial transport are being vigorously pursued on two fronts: (1) analytical and numerical studies of the dynamics of the IPOs independent of their origin, and (2) full nonlinear simulations of the boundary that study both IPO creation and dynamics. The work on dynamics[46–48] intends to provide an understanding of how the IPOs will transport particle and heat in the SOL without getting involved in the physics of their creation while nonlinear modeling work,[49–52] such as that by the code BOUT, tries to address the issue of IPO formation and transport and the nonlinear interaction of the IPOs with the background plasma and each other. The analytical work has made successful predictions such as typical IPO radial velocities and fluxes and the IPO density and temperature decay [Eqs. (1) and (2)]. Output from the BOUT code for *L*-mode conditions has been analyzed and compared to probe data. The simulation features very strong intermittency and radial profiles of the skewness of the density were computed, as shown in Fig. 11, for two density cases [$\langle n_e \rangle / n_{GW} = 0.25$ (in red) and $\langle n_e \rangle / n_{GW} = 0.5$ (in black)]. The agreement with the experimental skewness shown Fig. 3 is quite remarkable, featuring the crossing of zero at the LCFS and the signature of negative IPOs slightly inside the LCFS. Thus, although in an early stage, the study of edge/SOL intermittency is progressing rapidly.[53]

VII. CONCLUSIONS

Intermittency is present in the boundary of the DIII-D tokamak in both *L*- and *H*-mode discharges, as indicated by data from various diagnostics. Structures featuring higher density and temperature than the surrounding plasma originate at or near the LCFS and travel radially in the SOL, transporting particle and energy. Although the amplitude of the IPOs in *L* mode increases with density at the LCFS, they carry a fairly constant fraction (50%–70%) of the local density at all radii and densities measured. Furthermore, the IPOs feature higher temperature than the background plasma at the LCFS, but they thermalize within a short distance of the LCFS, in agreement with analytical predictions. In *L* mode, the IPO phenomenon is important in determining the structure of the SOL and it results in an enhanced plasma–wall contact. However, the presence of ELMs in *H* mode, carrying more energy and particles than the IPOs, transiently dominates the structure of the SOL and the plasma–wall interaction. The *H*-mode data for this work have been evaluated between ELMs.

ACKNOWLEDGMENTS

Discussions with K. H. Burrell, J. Terry, D. D'Ippolitto, and the technical support of L. Chousal and R. Hernandez are acknowledged.

This research was supported by the U.S. Department of Energy under Contract Nos. DE-AC03-99ER54463, DE-AC05-00OR22725, W-7405-ENG-48, and Grant Nos. DE-FG03-95ER54294, and DE-FG02-89ER53296.

[1] J. A. Boedo, D. Gray, L. Chousal *et al.*, Rev. Sci. Instrum. **69**, 2663 (1998).
[2] B. LaBombard, M. V. Umansky, R. L. Boivin, J. A. Goetz *et al.*, Nucl. Fusion **40**, 2041 (2000).
[3] M. R. Wade, W. P. West, R. D. Wood, S. L. Allen, J. A. Boedo, N. H. Brooks, M. E. Fenstermacher, D. N. Hill *et al.*, J. Nucl. Mater. **266–269**, 44 (1999).
[4] A. H. Nielsen, H. L. Pecsell, and J. Juul Rasmussen, Phys. Plasmas **3**, 1530 (1996).
[5] R. D. Lehmer, Ph.D. thesis, University of California Los Angeles, UCSD-ENG-032, 1996.
[6] E. Sanchez, C. Hidalgo, C. Riccardi, J. Bleuel, B. Carreras, D. E. Newman *et al.*, Phys. Plasmas **7**, 1408 (2000).
[7] B. K. Joseph, R. Jha, P. K. Kaw, S. K. Mattov *et al.*, Phys. Plasmas **4**, 4292 (1997).
[8] R. A. Moyer, R. D. Lehmer, T. E. Evans *et al.*, Plasma Phys. Controlled Fusion **38**, 1273 (1996).
[9] R. Jha and Y. C. Saxena, Phys. Plasmas **3**, 2979 (1996).

[10]B. Carreras, V. E. Lynch, D. E. Newman *et al.*, Phys. Plasmas **7**, 3278 (2000).
[11]B. A. Carreras, V. E. Lynch, and B. LaBombard, Phys. Plasmas **8**, 3702 (2001).
[12]W. Press, S. Teukolsky, W. Vettering, and B. Flannery, *Numerical Recipes in FORTRAN* (Cambridge University Press, Cambridge, 1986), p. 606.
[13]E. Sanchez, C. Hidalgo, D. Lopez-Bruna, I. Garcia-Cortes, R. Balbin *et al.*, Phys. Plasmas **7**, 1408 (2000).
[14]P. H. Rebut and B. E. Keen, Fusion Technol. **11**, 13 (1987).
[15]J. F. Lyon, B. A. Carreras, K. K. Chipley, M. J. Cole, J. H. Harris, T. C. Jernigan, R. L. Johnson, V. E. Lynch, B. E. Nelson, J. A. Rome *et al.*, Fusion Technol. **10**, 179 (1986).
[16]H. Renner, the WII-AS Team, the NBI Group, the ICF Group, and the ECRH Group, Plasma Phys. Controlled Fusion **37**, A53 (1995).
[17]A. V. Filippas, R. D. Bengtson, G. X. Li, M. Meier, CH. P. Ritz *et al.*, Phys. Plasmas **2**, 839 (1995).
[18]J. Soteckel, M. V. Heller, J. Petrzilka *et al.*, Phys. Plasmas **6**, 846 (1999).
[19]I. Garcia-Cortes, M. A. Pedrosa, C. Hidalgo, B. Branas, T. Estrada, R. Balbin, E. De la Luna, J. Sanchez, and A. P. Navarro, Phys. Fluids B **4**, 4007 (1992).
[20]E. Ascasibar, C. Alejaldre, J. Alonso, F. de Aragon, R. Balbin, B. Branas, E. de la Cal, F. Castejon, J. Castrejon, G. Catalan *et al.*, in *Plasma Physics and Controlled Nuclear Fusion Research, Proceedings of the 15th Conference on Plasma Physics and Controlled Nuclear Fusion Research, Seville* (IAEA, Vienna, 1995), Vol. 1, p. 749.
[21]I. Garcia-Cortes, R. Balbin, A. Loarte, J. Bleuel *et al.*, Plasma Phys. Controlled Fusion **42**, 389 (2000).
[22]B. LaBombard, R. L. Boivin, M. Greenwald *et al.*, Phys. Plasmas **8**, 2107 (2001).
[23]J. L. Terry *et al.*, J. Nucl. Mater. **290**, 757 (2001).
[24]S. J. Zweben, D. P. Stotler, J. L. Terry *et al.*, Phys. Plasmas **9**, 1981 (2002).
[25]I. H. Hutchinson, R. Boivin, F. Bombarda *et al.*, Phys. Plasmas **1**, 1511 (1994).
[26]S. J. Zweben and S. S. Medley, Phys. Fluids B **1**, 2058 (1989).
[27]J. A. Boedo, D. L. Rudakov, R. A. Moyer, S. Krasheninnikov *et al.*, Phys. Plasmas **8**, 4826 (2002).
[28]D. L. Rudakov, J. A. Boedo, R. A. Moyer, S. Krasheninnikov *et al.*, Plasma Phys. Controlled Fusion **44**, 717 (2002).
[29]J. A. Boedo, D. L. Rudakov, R. J. Colchin, D. G. Whyte, G. R. McKee, M. J. Schaffer *et al.*, "Intermittent convection in the boundary of DIII-D," to appear in J. Nucl. Mater.
[30]J. L. Luxon, Nucl. Fusion **42**, 614 (2002).
[31]J. L. Luxon and L. G. Davis, Fusion Technol. **8**, 441 (1985).
[32]J. G. Watkins, J. Salmonson, R. A. Moyer *et al.*, Rev. Sci. Instrum. **63**, 4728 (1992).
[33]D. L. Rudakov, J. A. Boedo, R. A. Moyer *et al.*, Rev. Sci. Instrum. **72**, 453 (2001).
[34]L. L. Lao *et al.*, Nucl. Fusion **25**, 1611 (1985).
[35]G. R. Tynan, J. Liberati, P. Pribyl, R. J. Taylor, and B. Wells, Plasma Phys. Controlled Fusion **38**, 1301 (1996).
[36]G. R. Tynan, L. Schmitz, R. W. Conn, R. Doerner, and R. Lehmer, Phys. Rev. Lett. **68**, 3032 (1992).
[37]G. R. Tynan, L. Schmitz, L. Blush, J. A. Boedo *et al.*, Plasma Phys. Controlled Fusion **36**, 285 (1994).
[38]G. R. Tynan, L. Schmitz, H. Kugel *et al.*, Phys. Plasmas **1**, 3301 (1994).
[39]R. A. Moyer, K. H. Burrell, T. N. Carlstrom, S. Coda *et al.*, Phys. Plasmas **2**, 2397 (1995).
[40]K. W. Gentle, Nucl. Technol./Fusion **1**, 479 (1981).
[41]T. L. Rhodes, C. P. Ritz, and R. D. Bengtson, Nucl. Fusion **33**, 1147 (1993).
[42]H. Tsui, A. Wooton, R. Bengtson *et al.*, Plasma Phys. Controlled Fusion **2**, 673 (1993).
[43]G. H. Wolf and the TEXTOR Team, J. Nucl. Mater. **122&123**, 1124 (1984).
[44]J. A. Boedo, D. Gray, S. Jachmich, R. Conn *et al.*, Nucl. Fusion **40**, 209 (2000).
[45]J. A. Boedo, P. W. Terry, D. Gray *et al.*, Phys. Rev. Lett. **84**, 2630 (2000).
[46]S. Krasheninnikov *et al.*, *Fusion Energy 2002, Proceedings of the 19th International Conference Lyon, France, 2002* (IAEA, Vienna, 2002) CD-ROM.
[47]S. Krasheninnikov, Phys. Lett. A **283**, 368 (2001).
[48]D. A. D'Ippolito, J. R. Myra, and S. I. Krasheninnikov, Phys. Plasmas **9**, 222 (2002).
[49]X. Xu, W. M. Nevins, R. H. Cohen, J. R. Myra, and P. B. Snyder, New J. Physics **4**, 53.1 (2002).
[50]P. Ghendrih, Y. Sarazin, C. Clement *et al.*, *Fusion Energy 2002, Proceedings of the 19th International Conference, Lyon, France, 2002* (IAEA, Vienna, 2002), CD-ROM.
[51]Y. Sarazin, X. Garbet, P. Ghendri, P. Beyer, and S. Benkadda, Theory of Fusion Plasmas, Proceedings of the Joint Varenna-Lausanne International Workshop, Soc. Italiana di Fisica, 1999, pp. 3–17.
[52]Ph. Ghendrih, Y. Sarazin, G. Attuel, S. Benkadda, and X. Garbet, "Theoretical analysis of long range turbulent transport in the scrape-off-layer," to be published in Nucl. Fusion.
[53]R. Maqueda, G. Wurden, S. Zweben *et al.*, Rev. Sci. Instrum. **72**, 931 (2001).